Motion Artifact Compensation in CT

Detlef Zerfowski

Institut für Algorithmen und Kognitive Systeme,
Universität Karlsruhe, Germany,
Email: zerfowsk@ira.uka.de

ABSTRACT

A new method for compensating motion artifacts in computerized tomography is presented. The algorithm operates on the raw data, that is, on the measured Radon transform. An edge detection is performed on the Radon transform image. Two curves are obtained from these edges, which are fitted by a polynomial. The pointwise differences between the edges of the Radon transform image and the fitted curves are used to determine the parameters for the motion compensation. The corresponding operations are performed on the rows of the Radon transform. Our method is independent of the image reconstruction algorithms like filtered backprojection, Fourier method, etc. since all transformations are performed on the raw data.

Keywords: Computerized tomography, Radon transform, motion artifacts, image preprocessing.

1. INTRODUCTION

In computerized tomography, patient motions play a significant role in the loss of image quality. Therefore, one is interested in methods which are able to compensate or to even eliminate motion artifacts in images for diagnostic purposes.

Due to special scan situations different kinds of motion have to be considered. E.g. in the case of incooperative patients like children, translations and rotations of the scanned region occure. In contrast to these relatively fast motions, respiration represents a more regular, slower, but also more complex motion, because of the deformation of the scanned object.

Several different methods have been proposed to reduce motion artifacts. One of these methods is to decrease scan time, but this results in a decrease of the signal to noise ratio. Therefore the resolution and image quality decrease, too.

Another method tries to suppress the patient motion. Here the patient has to be fixed or has to be extremely cooperative. E.g. the patient is only allowed to breath during special time intervals only. Both situations are very uncomfortable for the patient.

For periodical motions a motion driven scan process has been proposed. Here the idea is to perform each scan in the same phase of motion (e.g. in the dead center of respiration). Obviously this approach needs additional hardware for monitoring the motion and is restricted to periodical motions.

An algorithmic approach is described by Helenon[1] et al. The authors tried to eliminate motion artifacts in reconstructed images. Regions of the image containing artifacts are identified manually. Afterwards parts of the image are filtered in the spectral domain using a two-dimensional fast Fourier transform and filters. One of the main disadvantages of this approach is that local compensations introduce new artifacts at the borders of the sub images.

Recently, Crawford et al.[2] proposed a model based method. There the respiration in an object cross section is modelled by time-varying magnification and displacement along two axes. This leads to an adapted filtered backprojection algorithm. In Ritchie et al.[3] the authors have refined the method in the sense that the motion model is assumed to be correct only in a small region around each object pixel. These assumptions lead to a pixel-specific backprojection algorithm.
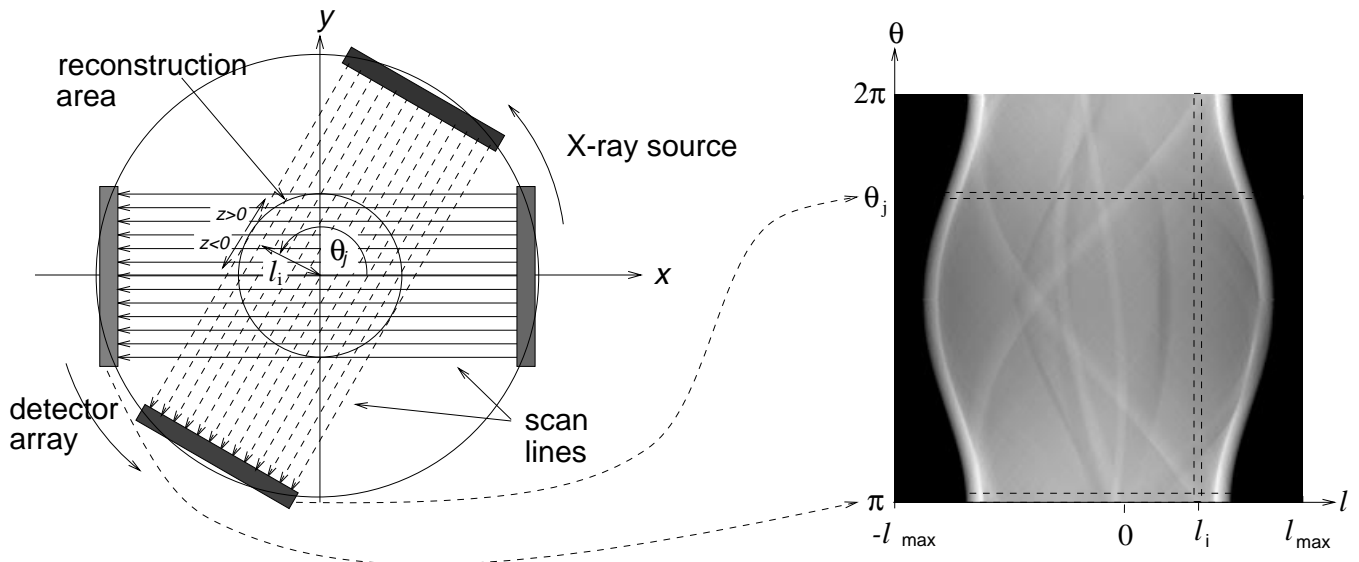
Figure 1. Geometrical interpretation of the Radon transform.

In contrast to the previously mentioned methods we propose a more pragmatic approach. During the reconstruction process, motion information which is highly localized in the raw data is spread over the complete image. Hence we do not operate on reconstructed images but on the measured Radon transform. The method does not need any additional hardware, e.g. for monitoring the motion, nor any modification of subsequent reconstruction algorithms.

We now use elementary properties of the Radon transform. As the convex hull of the object part lying in the slice to be scanned characterizes the shape of the corresponding Radon transform, this information can be used to improve the image.

In a first step the shape of the scanned Radon transform is determined. Afterwards the edges of this transform are fitted to an adequate shape using polynomials of degree four. After rescaling the corresponding rows of the Radon transform an arbitrary reconstruction algorithm can be performed to obtain an improved image.

In the next section we briefly describe the Radon transform, its geometrical interpretation, and elementary properties. Afterwards the influence of motion on the Radon transform is analyzed and some examples corresponding to different kinds of motions are given. Then we will describe the operations on the Radon transform which have to be performed for motion compensation. Finally, the improvement of image quality is evaluated and shown by the given examples.

2. THE RADON TRANSFORM AND ITS PROPERTIES

The well known Radon transform maps a spatial function (in computer tomography (CT) the spatial absorption coefficient) by the line integrals over all possible scan lines to an image as shown in Figure 1. In the two dimensional case of CT the coordinates of the transformed space are the distance l of the lines from the origin and the angle θ between the perpendicular of the line and the x-axis (see Figure 1). The function value at position (l, θ) is determined by the corresponding line integral (cf. Herman,[4] Cho et al.[5])

$$[\mathcal{R}f](l, \theta) = \begin{cases} \int\limits_{-\infty}^{\infty} f(\sqrt{l^2 + z^2}, \theta + \tan^{-1}(\frac{z}{l}))dz & \text{if } l \neq 0, \\ \int\limits_{-\infty}^{\infty} f(z, \theta + \frac{\pi}{2})dz & \text{if } l = 0. \end{cases} \tag{1}$$

During a CT scan a set of parallel line integrals with angles θ_i through an object slice is measured. It should be mentioned that the following discussion also holds for other scanner geometries like fan beam scanners, because the
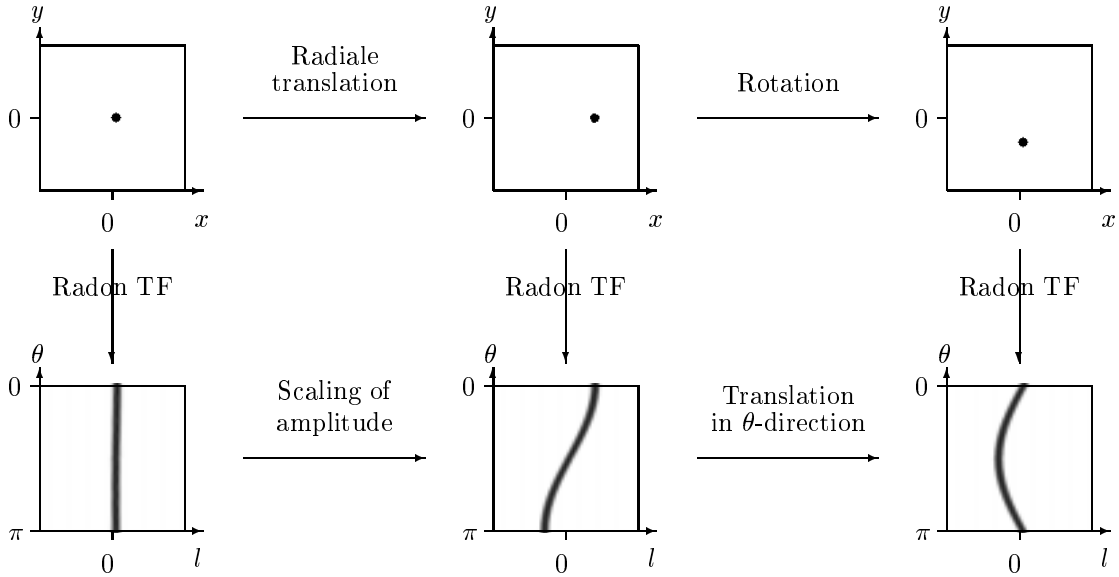
Figure 2. Correspondences between image domain and Radon transform domain.

measured data sets can be rearranged and interpolated using rebinning methods to obtain data sets corresponding to parallel beam data.

A data set from one projection (i.e. fixed θ) is represented by one row in the Radon transform as in Figure 1. Performing several of these measurements by incrementing the angle θ yields a two dimensional representation of the Radon transform.

Since our approach of motion artifact compensation operates on the Radon transform we recall some of its elementary properties. First we consider the translation invariance

$$[\mathcal{R}f](l, \theta) = [\mathcal{R}f](l, \theta + 2\pi) = [\mathcal{R}f](-l, \theta + \pi) \tag{2}$$

in the transform domain, which can be easily verified by Equation 1. Geometrically, Equation 2 describes the fact that after rotation of the scanner by 2π the measurements should be the same. A rotation by π would also yield no new information because the integration along lines with distance l would be performed in the opposite direction of the lines with corresponding negative distance to the origin. For this reason it is only necessary to measure the Radon transform for angles in the interval $(0, \pi]$. Furthermore, Equation 2 show that the rotation of the object corresponds to a translation of the Radon transform along the θ-axis.

For further discussion, we take a look at a point in the spatial domain and its image in the transformed domain. Because of Equation 1, an object point with distance d from the origin is distributed in the Radon transform on a sine curve with "amplitude" d. This is also obvious geometrically because no scan line with coordinate $l > d$ can pass through this object point. Therefore, translating points in the spatial domain changes the amplitude of the corresponding sine curve in the transformed domain.

3. SHAPES OF RADON TRANSFORMS

Instead of single object points we now consider the shape of the Radon transform of more complex objects. Since in every row of the Radon transform the leftmost and rightmost values correspond to the integrals of the lines which just touch the object these values represent the convex hull of the scanned object.

For objects with elliptical convex hulls the shapes of their Radon transforms can easily be determined (cf. Kak and Slaney[6]). An ellipse with half axis a and b given, centered in the origin is assumed. The distances $d(\theta)$ between the origin and the tangents at the ellipse describe the shape of the corresponding Radon transform. To express these distances in θ, one has to solve the following system of three equations:
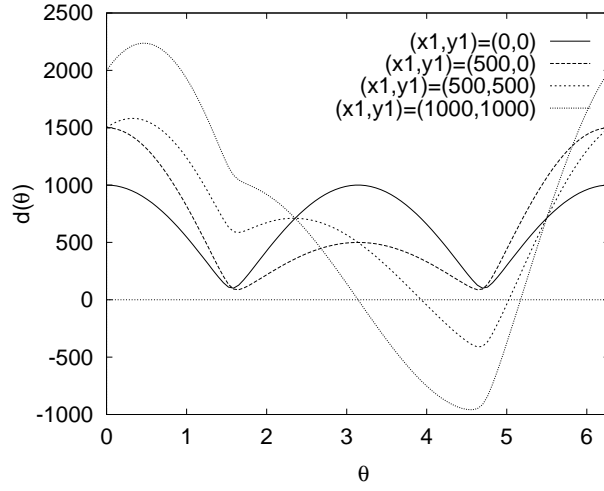
Figure 3. Edge curves $d(\theta)$ of an elliptical objects with half axis $(a, b) = (1000, 100)$, translated into (x_1, y_1) with $0 \le \theta < 2\pi$.

- Equation of ellipse

$$\frac{x^2}{a^2} + \frac{y^2}{b^2} = 1, \tag{3}$$

- Hesse's normalform of tangents

$$x \cdot \cos(\theta) + y \sin(\theta) = d, \tag{4}$$

- Equality for derivation of Equation 3 and known slopes of the tangents

$$y' = -\frac{b^2 x}{a^2 y} \overset{!}{=} -\frac{\cos(\theta)}{\sin(\theta)}. \tag{5}$$

This system of equations leads to

$$d(\theta)^2 = a^2 \cos^2(\theta) + b^2 \sin^2(\theta). \tag{6}$$

The main idea in the upcoming algorithm is to fit the two edges of the measured Radon transform to equations of a form similar to Equation 6. This equation is only valid for non-rotated, elliptical objects centered at the origin. Rotation by an angle α results in an additional offset $-\alpha$ to the viewing angle θ.

Translation of the elliptical object leads to a more complicated expression. If we allow the object to ly at an arbitrary position (x_1, y_1) with rotation angle α, the system of equations 3 - 5 changes to

$$1 = \frac{(x - x_1)^2}{a^2} + \frac{(y - y_1)^2}{b^2}, \tag{7}$$

$$d(\theta) = x \cdot \cos(\theta - \alpha) + y \sin(\theta - \alpha), \tag{8}$$

$$y' = -\frac{\cos(\theta - \alpha)}{\sin(\theta - \alpha)} \tag{9}$$

and Equation 6 becomes

$$d(\theta) = x_1 \cos(\theta - \alpha) + y_1 \sin(\theta - \alpha) + \sqrt{a^2 \cos^2(\theta - \alpha) + b^2 \sin^2(\theta - \alpha)}. \tag{10}$$

Figure 3 shows the edge curves of elliptical objects under different translations.

In each row of the measured data the l-coordinate of the leftmost and rightmost values above a chosen threshold has to be determined. The threshold is being necessary to ignore the background noise. We have to interpret these coordinates as samples of the two edge curves $d_{\text{left}}(\theta)$ and $d_{\text{right}}(\theta)$, respectively.
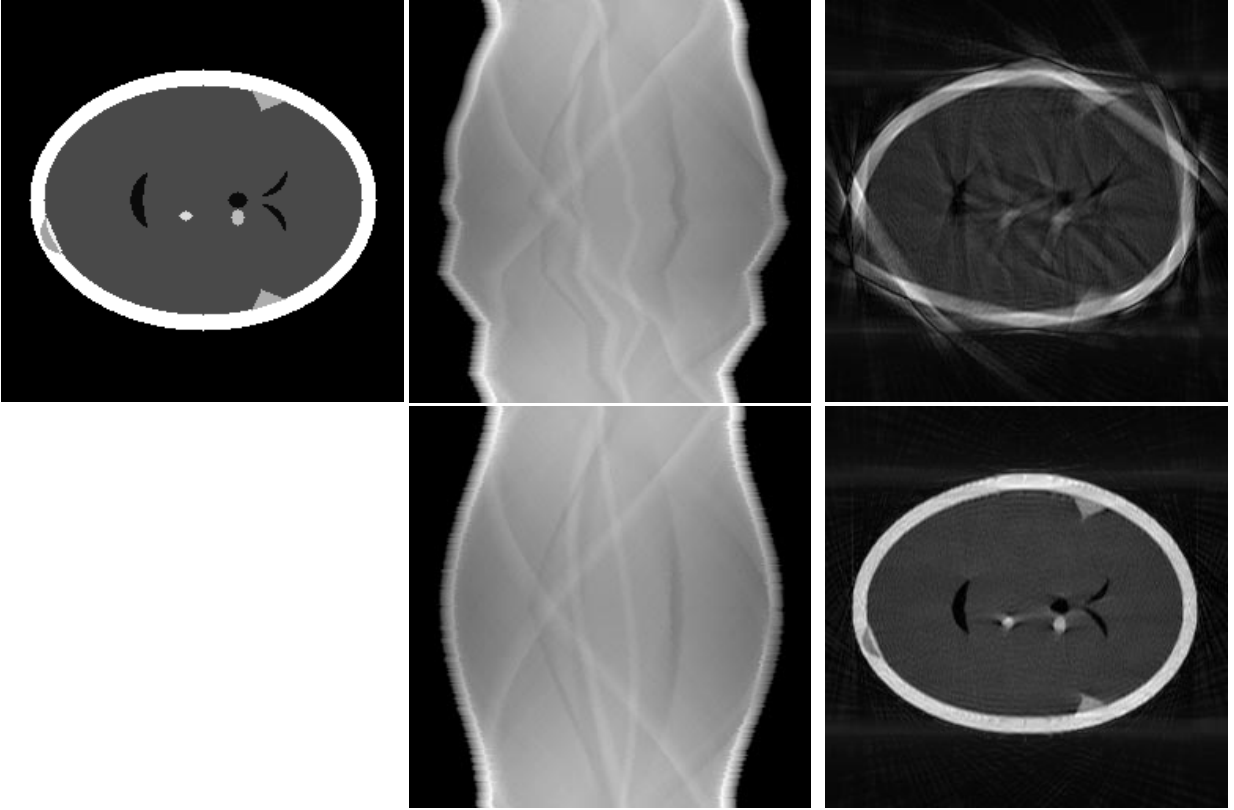
Figure 4. Top row: Phantom (left), Radon transform of the periodically translated phantom (center) and corresponding reconstruction (right). Bottom row: Modified Radon transform and reconstruction.

Before fitting the two curves, one has to consider how different kinds of motion influence these curves. First, we take a look at simple translations of the object during the scan process. In Figure 4 the Radon transform of a phantom is shown, which has been periodically translated in radial direction. The corresponding reconstruction at the upper right shows severe artifacts.

Note that the distance between the two curve points in a row do not depend on the movement of the object. Each row in the Radon transform (upper center of Figure 4) needs to be translated to the corresponding positions as in Figure 1. With Equation 6, this can be done by fitting the curves $d_{\mathrm{left}}(\theta)$ and $d_{\mathrm{right}}(\theta)$ by a linear combination of sine and cosine terms as given in Equation 6, which result in two modified curves $d'_{\mathrm{left}}(\theta)$ and $d'_{\mathrm{right}}(\theta)$. For each row in the Radon Transform, i.e. for each value of θ we therefore obtain values

$$
\begin{aligned}
\Delta_{\mathrm{left}}(\theta) &:= d'_{\mathrm{left}}(\theta) - d_{\mathrm{left}}(\theta) \quad \text{and} \\
\Delta_{\mathrm{right}}(\theta) &:= d'_{\mathrm{right}}(\theta) - d_{\mathrm{right}}(\theta)
\end{aligned}
\tag{11}
$$

representing the shifts, which have to be performed in the corresponding rows. In the special case of radially translated objects we have

$$
\Delta_{\mathrm{left}}(\theta) = \Delta_{\mathrm{right}}(\theta)
\tag{12}
$$

due to the translation property of the Radon Transform (see Figure 2).

In general the occurring movements differ from the one just described and Equation 12 does not hold any more. In particular we cannot compensate respiration artifacts in this simple manner. In Figure 6 we give a Radon transform of a respiration like movement, which is based on a model given by Ritchie[3] et al., and the corresponding reconstructed image without any artifact compensation.
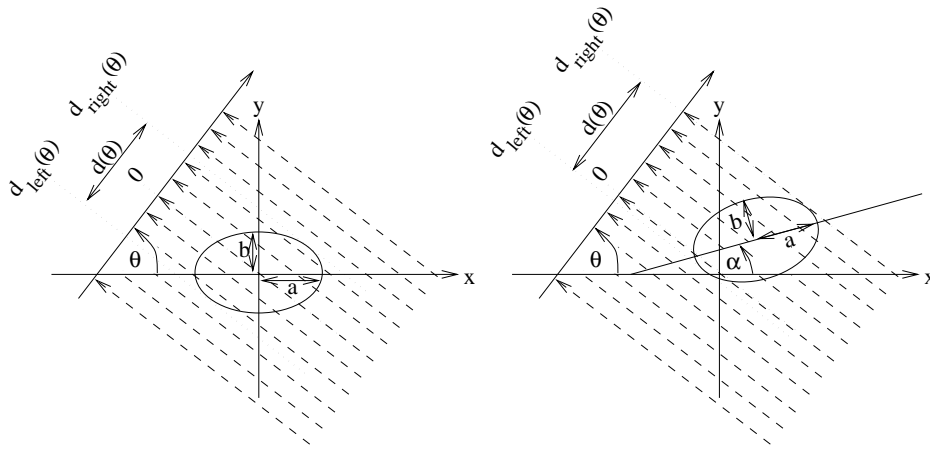
Figure 5. Projection of an elliptical object lying in the coordinate center (left), and in an arbitrary position (right).

4. FITTING OF THE EDGES

Now we consider the problem of fitting the data points $d_{\text{left}}(\theta)$ and $d_{\text{right}}(\theta)$ to functions using the method of general linear least squares (cf. Press[7] et al.), which estimates the coefficients of a linear equation

$$d'(\theta) = \sum_{k=0}^{M-1} a_k \Theta_k(\theta), \tag{13}$$

with a set of arbitrary chosen basis functions $\Theta_k(\theta)$. If one chooses $\cos^2(\theta)$ and $\sin^2(\theta)$ as basis functions for fitting $d(\theta)^2$ according to Equation 6 this would lead to a reconstructed object with elliptical convex hull. Therefore one has to choose basis functions which do not imply such restrictions to the shape of the object. This is achieved by the use of polynomials in θ for the fitting process.

We now consider one tangent and their distance to the origin while scanning a simulated abdominal region without respiration. As shown on the left hand side of Figure 5 we start with a horizontal view (i.e. $\theta = \frac{\pi}{2}$). In this situation, the tangent passes the origin with distance $d_{\text{right}}(\frac{\pi}{2})$. During anti-clockwise scanner rotation the distance increases to a maximum in the vertical scanner position ($\theta = \pi$), since the corresponding vertical tangent touches the left side of the object, which is the outermost part of the body. Further rotation decreases $d_{\text{right}}(\theta)$ until $\theta = \frac{3\pi}{2}$ corresponding to the opposite of the starting position. Since the distance varies smoothly during this half rotation $d_{\text{right}}(\theta)$ (and $d_{\text{left}}(\theta)$ respectively) contains two turning points over an interval of length π (cf. Figure 3). Obviously polynomials which have to fit the distance functions have to be at least of degree four. Since polynomials of higher degree may result in fitted curves with more than two turning points we only consider polynomials of degree four and Equation 13 becomes

$$d'(\theta) = \sum_{k=0}^{4} a_k \theta^k. \tag{14}$$

Furthermore we have to take into account, that the sampled values $d_{\text{right}}(\theta)$ are not equally influenced by the motion. E.g. in vertical scanner position the displacement of the right tangent due to motion is much less than in the starting position $\theta = 0$. We therefore have to give some constraints on how far we may translate the sampled values $d_{\text{right}}(\theta)$ and $d_{\text{left}}(\theta)$. Especially in the scanner position $\theta = \pi$ the distance $d_{\text{left}}(0)$ can be considered constant in time, since it represents the distance of the table on which the patient is lying. On the other hand, in the same scanner position $d_{\text{right}}(0)$ has the strongest variation in time. In vertical scanner position, the effect of respiration on $d_{\text{right}}(\pi)$ and $d_{\text{left}}(\pi)$ can be assumed to be equal. Thus we can regard the curve data as having different "uncertainties" in different regions. In the fitting algorithm we therefore prescribe different standard deviations σ_i

to the values $d_i := d(i \cdot \Delta\theta)$, ($i \in \mathbf{N}$ and $\Delta\theta$ denotes the difference between two discrete view angles). To estimate the coefficients a_i in Equation 13 one uses a merit function

$$\chi^2 = \sum_{i=1}^{N} \left(\frac{d_i - \sum_{k=1}^{M} a_k \Theta_k(\theta_i)}{\sigma_i} \right)^2 , \tag{15}$$

which has to be minimized. Here N represents the number of viewing angles (i.e. the number of rows in the Radon transform) and σ_i is the standard deviation of the i-th data point and can be chosen as

$$\sigma_i = \sin\left(i\frac{\pi}{N}\right). \tag{16}$$

To avoid singular matrices during the estimation process it is recommended to estimate the coefficient vector $\vec{a} = (a_0, \ldots, a_{M-1})$ using a singular value decomposition method.

5. EXAMPLES

In this section different kinds of motion are modelled and simulated. For the simulation of the CT scan, a software package called **TomAS** (cf. Zerfowski[8] et al.) is used. Besides elementary image manipulating functions and a large set of signal transform algorithms, this tool offers an interface to simulate different scanner geometries (e.g. fan or parallel beam scanner with different increments of the rotation angle θ and different numbers of detectors). The software is not limited to a special class of phantoms. A variety of different reconstruction methods including filtered back-projection, Fourier reconstruction, convolutional reconstruction and algebraic reconstruction techniques is implemented.

The simulation of motion has been done by modifying the phantom during the scan process. In Figure 4 the phantom has been placed in a parallel scanner with 256 detectors performing 256 scans for $0 \leq \theta < \pi$. A reconstruction diameter of 30 cm with its origin in the center of the image is assumed. The periodical translation is simulated by moving the phantom to the pixel coordinates (x, y) with $x = y = 5 - |(i + 5 \bmod 20) - 10|$ during the i-th projection. Therefore this is a uniform translation between the coordinates $(-5, -5)$ and $(5, 5)$. In reality these points would have a distance of about 16 mm.

In contrast to the previously described motion, respiration is a deforming motion. In Figure 6 the complete compensation process for a simulated respiration is visualized. Given the phantom $f(x, y)$ the used motion model (taken from Crawford[2] et al.) describes the time-varying phantom $f'(x, y, t)$. According to a situation where the patient is lying on a table, the patient's back can be assumed not to move. In the motion model this can be considered by choosing an appropriate fix point (x_F, y_F) of the motion. Normally this should be the center of the patient table.

The time-varying phantom can now be described by (cf. Figure 6)

$$f'(x, y, t) = f(x_F \alpha_x(t) + x\beta_x(t), y_F \alpha_y(t) + y\beta_y(t)) \text{ with} \tag{17}$$

$$\begin{array}{ll}
\alpha_x(t) = 1 - \frac{1}{m_x(t)}, & \alpha_y(t) = 1 - \frac{1}{m_y(t)}, \\
\beta_x(t) = \frac{1}{m_x(t)} & \text{and} \quad \beta_y(t) = \frac{1}{m_y(t)}.
\end{array} \tag{18}$$

The magnification in x- and y-direction are given by

$$m_x(t) = 1 - \frac{\sin(\theta)}{s_x} \quad \text{and} \tag{19}$$

$$m_y(t) = 1 + \frac{\sin(\theta)}{s_y}. \tag{20}$$

The choice of $m_x(t)$ and $m_y(t)$ causes an expansion in x-direction with a simultaneous contraction in y-direction and vice versa. The constant scale parameters s_x and s_y represent the maximal contraction and expansion in the corresponding direction.
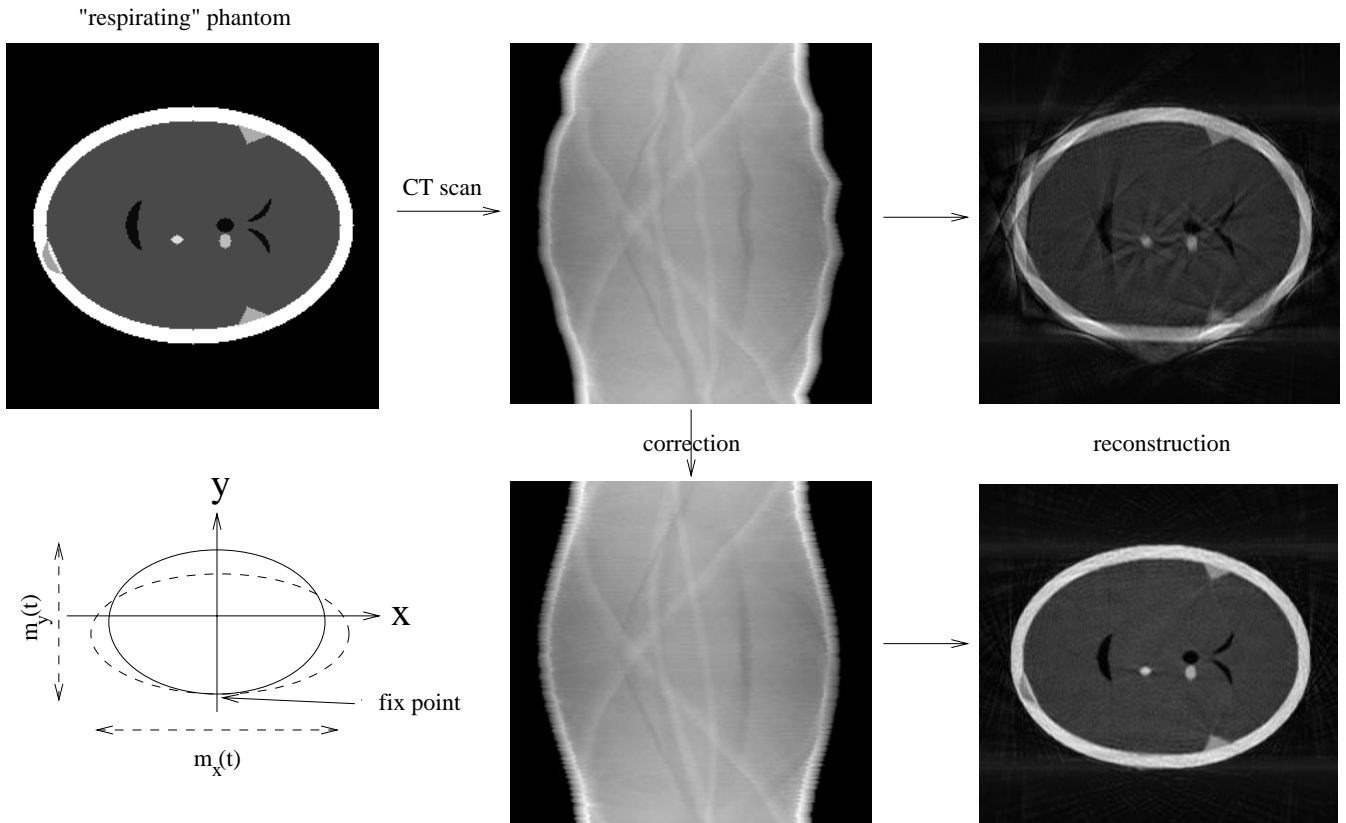
Figure 6. Respiration model and compensation of respiration-like motion artifacts.

In the upper row of Figure 6 the Radon transform of the respirating phantom (center) and its corresponding reconstruction (right) are given. In particular the middle of the right edge curve of the Radon transform is much more jagged than the left curve. The central part of the left curve is nearly undisturbed. This originates from the fact, that these values correspond to scan lines of the projection in the neighborhood of the fix point of motion. The jagged part of the right curve corresponds to scan lines tangent to strongly moving object parts.

In the reconstruction (upper right) typical streaking artifacts decrease the image quality (cf. Figure 4 for the translated phantom). Some structures of the phantom are not visible, especially in the outer left part. Therefore, this information about perhaps pathological structures are not available for diagnostics.

In the lower row of Figure 6 the modified Radon transform (center) is given using the above described compensation method. On the lower right the corresponding reconstruction is shown using the same reconstruction algorithm as before. A dramatical increase of image quality can be observed. The streaking artifacts have been eliminated. All structures of the phantom are clearly visible and can be considered for diagnostic purposes.

We want to stress again that the described compensation method is an image preprocessing step, which is independent of the reconstruction technique performed afterwards.

6. CONCLUSION

In this paper we have presented a new algorithm for motion artifact compensation in CT. The method is suitable for different kinds of motions. The algorithm operates on the measured Radon transform and results in a modified Radon transform. Since these modified data can be reconstructed by arbitrary algorithms the described compensation method is an image preprocessing. Therefore the algorithm is suited to be implemented on tomographic equipement already in use.

REFERENCES

1. O. Helenon, D. S. Chanin, L.-J. M., and J. Frija, "Artifacts on Lung CT scans: Removal with Fourier Filtration," *Radiology* **171**, pp. 572–574, 1989.
2. C. R. Crawford, K. F. King, C. J. Ritchie, and J. D. Godwin, "Respiratory Compensation in Projection Imaging Using a Magnification and Displacement Model," *IEEE Transactions on Medical Imaging* **15**, pp. 327–332, June 1996.
3. C. J. Ritchie, C. R. Crawford, K. F. Godwin, J. D. King, and Y. Kim, "Correction of Computed Tomography Motion Artefacts Using Pixel-Specific Back-Projection," *IEEE Transactions on Medical Imaging* **15**, pp. 333–342, June 1996.
4. G. T. Herman, *Image reconstruction from projections*, Academic Press, 1980.
5. Z. H. Cho, J. P. Jones, and M. Singh, *Foundations of Medical Imaging*, John Wiley & Sons, Inc., 1993.
6. A. C. Kak and M. Slaney, *Principles of Computerized Tomography*, New York: IEEE Press, 1987.
7. W. H. Press, S. A. Teukolsky, W. T. Vetterling, and B. P. Flannery, *Numerical Recipes in C*, Cambridge University Press, 2 ed., 1992.
8. D. Zerfowski, T. Rohlfing, U. Mende, and T. Beth, "TomAS – Tomographic Algorithms and Ultrasound Simulation," in *CAR '97*, Lemke, ed., p. 1017, Elsevier Science, 1997.